NJC

Accepted Manuscript

New Journal of Chemistry

Dynamic Article Links ▶

ARTICLE TYPE

Two novel aggregation-induced emission active coumarin-based Schiff bases and their applications in cell imaging

Hongde Xiao[a], Kun Chen[a], Dandan Cui[b], Nannan Jiang[b], Gui Yin[a]*, Jie Wang, and Ruiyong Wang[b]*

Two new coumarin-based Schiff bases, 8,8'-((1E,1'E)-hydrazine-1,2-diylidenebis(methanylylidene))bis(7-hydroxy-4-methyl-2H-chromen-2-one), short for CHC, and 7-hydroxy-8-((E)-((E)-((2-hydroxynaphthalen-1-yl)methylene)hydrazono)methyl)-4-methyl-2H-chromen-2-one, short for CHN, with excited-state intramolecular proton-transfer (ESIPT) property, were synthesized and characterized. Both of the compounds displayed aggregation-induced emission (AIE) characteristic, of which CHC nanoparticles emitted reddish
10 orange fluorescence while CHN nanoparticles exhibited saffron yellow fluorescence. The appearances of emission peaks in the long wave regions with large Stokes-shifts demonstrated the occurrences of the ESIPT process. Observations of the nanoparticles' morphologies were undertaken through a transmission electron microscope (TEM) method. Furthermore, due to the good biocompatibilities, high stabilities and the large Stokes-shifts, the two compounds were ideal candidates for cell staining.

Introduction

15 During the past decades, efficient organic fluorescent materials have been arising considerable research interests due to their potential applications including the organic light-emitting diodes (OLED),[1] organic field effect transistors (OFET),[2] fluorescent
20 sensors,[3] photovoltaic cells,[4] fluorescent biological labels,[5] organic lasers,[6] etc. Although many traditional organic fluorophores with large delocalized π-conjugated moieties emit strongly in their dilute solutions, the emissions become weak at high concentrations or in aggregated states,[7] which is known as
25 concentration quenching or aggregation-caused quenching (ACQ). The reason is believed to be that the excited states of the aggregates often decay via non-radiative pathways caused by strong intermolecular vibronic interactions such as exciton coupling and excimer formation in the solid state.[8] The notorious
30 ACQ effect has greatly limited the efficiency of the organic fluorescent materials because in the practice, those materials are commonly used in the solid state. Various approaches, such as the encapsulation by amphiphilic surfactants and blending with transparent polymers,[9] have been taken to prevent the aggregating
35 but have met with only limited success.

H. D. Xiao, K. Chen, G. Yin, J. Wang
State Key Laboratory of Analytical Chemistry for Life Science,
School of Chemistry and Chemical Engineering,
40 Nanjing University,
Nanjing 210093, People's Republic of China
E-mail: yingui@nju.edu.cn

D. D. Cui, N. N. Jiang, R. Y. Wang
45 School of Life Science, Nanjing University,
Nanjing, 210093, China
Email: wangry@nju.edu.cn

Fortunately, materials displaying aggregation-induced emission
50 (AIE) characteristics can be used to tackle this thorny problem nicely. Since the first AIE compound, 1-methyl-1,2,3,4,5-pentaphenylsiole, was synthesized by Tang's group,[10] several organic compounds based on different fluorophores have been reported to display AIE characteristics, such as 1-cyano-*trans*-
55 1,2-bis-(4'-methylbiphenyl)ethylene (CN-MBE),[11] diphenyldibenzofulvene (DPDBF) derivatives,[12] rhodanineacetic acid-pyrene derivative (RAAP),[13] whose potential applications were further investigated in the fields of bio/chem sensor,[14] cell imaging[15] and optoelectronic devices.[16]
60

In recent years, a few interpretations of AIE in terms of the intra- and intermolecular effects have been reported. Intramolecular effects on fluorescence enhancement are simply explained by the conformational changes from the twisted conformations to the
65 planar ones. The planar conformations are favourable for the radiation process.[17] Intermolecular interactions are related with the specific aggregation morphology (H-type and J-type aggregation). H-aggregates tend to induce the nonradiative deactivation process, whereas, J-aggregates induce a relatively
70 high fluorescence efficiency.[18]

As far as the specific emission properties are concerned, the excited-state intramolecular proton-transfer (ESIPT) process could have a great contribution to fluorescent emission of the
75 chromophore in solid state. The planar conformations are beneficial to both AIE and ESIPT. The ESIPT dyes can present a large Stokes shift caused by transformation of the excited enol form (E*) to the excited proton-transferred keto form (K*), diminishing the self-absorption to a great extent. This property
80 enables the ESIPT compounds a wide range of applications in systems such as fluorescent probes,[19] laser dyes,[20] organic electroluminescence optical materials,[21] scintillators,[22] as well as in solar collectors.[23]

In general, an ESIPT mechanism involves a proton transfer from the donor to the acceptor moiety.[24] The most common ESIPT donor is the phenolic OH, and the basic group is usually a heteroatom, such as carbonyl oxygen or nitrogen atom on amide.

5 And in terms of AIE compounds structures, the molecules have been found to be associated with aromatic groups with rotatable C-C, C-N or N-N single bond.[25] Due to the superior light stability, high fluorescent quantum yield, as well as the good biocompatibility, courmarin derivatives become ideal candidates

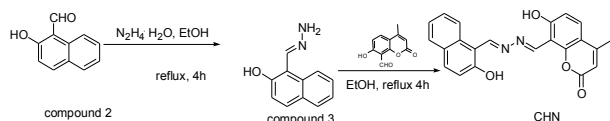10 for fluorescent biological materials. These factors motivated us to design and synthesize two novel coumarin-based ESIPT compounds, 8,8'-((1E,1'E)-hydrazine-1,2-diylidenebis(methanylylidene))bis(7-hydroxy-4-methyl-2H-chromen-2-one), short for CHC, and 7-hydroxy-8-((E)-((E)-((2-

15 hydroxynaphthalen-1-yl)methylene)hydrazono)methyl)-4-methyl-2H-chromen-2-one, short for CHN. And their nanoparticles were prepared by a simple reprecipitation method without using surfactants. What's more, biocompatibility and the cell uptake behavior of the nanoparticles were investigated to evaluate their

20 potential applications in cell imaging.

Experiment

compound 1

N2H4·H2O, EtOH
reflux, 4h

CHC
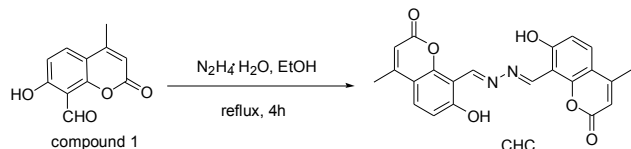
25   Scheme 1. Synthesis of CHC

compound 2

N2H4·H2O, EtOH
reflux, 4h

compound 3

EtOH, reflux 4h

CHN

Scheme 2. Synthesis of CHN

Reagents, Materials and Equipments

30

All of the reagents were of analytical grade unless otherwise noted. ^{1}H-NMR spectra were recorded on Bruker Ultrashield 300 MHz NMR spectrometer. Chemical shifts were expressed in ppm (in DMSO-d_6 or CDCl$_3$; TMS as an internal standard) and

35 coupling constants (J) in Hz. Mass spectroscopy was obtained from Thermo LCQ Fleet MS spectrometer in negative ion mode. Differential scanning calorimetry (DSC) and thermal gravimetric analysis (TGA) were investigated on Netzsch STA 449 C. UV-vis absorption and fluorescence spectra were measured using Perkin

40 Elmer Lambda 35 spectrophotometer and Perkin Elmer LS-55 spectrophotometer respectively. Transmission Electron Microscopy (TEM) images were recorded on JEX-2100 transmission electron microscopy. Fluorescence Microscope photos of nanoparticles and cell imaging were captured by

45 Olympus FV-1000 laser scanning confocal fluorescence microscope.

Synthesis of compound 2

Compound 2 was synthesized according to our previous
50 procedures.[26]

Synthesis of 7-hydroxy-4-methyl-coumarin

4-Methylbenzenesulfonic acid (5 g) was added into the solution of resorcinol (11.0 g, 0.1 mol) in toluene (40 mL), and then
55 acetoacetic ester (13.0 g) was added drop wise. The reaction mixture was refluxed for 3 h and monitored by TLC until the resorcinol was completely consumed. After cooling, the solution was poured into ice water (100 mL), yellow precipitate was collected by filtration and washed with cold water. Pale yellow
60 solid was obtained by recrystallization with 95% ethanol (11.3 g, Yield: 64 %). M.p. 185.0~186.0 ^{o}C. ^{1}H NMR (300 MHz, CD$_3$OD), δ=7.61 (d, 1H, J = 8.9 Hz), 6.83 (d, 1H, J = 10 Hz), 6.70 (s, 1H), 6.10 (s, 1H), 2.42 (s, 3H). TOF MS EI calcd 176.0, found 176.0.

65

Synthesis of compound 1[27]

7-Hydroxy-4-methyl-coumarin (5.3 g, 0.03 mol) and hexamine (9.8 g, 0.07 mol) in glacial acetic acid (50 mL) were refluxed for 5.5 h, and then 20% HCl (75 mL) was added and the solution was
70 heated for 1 h. After cooling, the reaction mixture was extracted with ether, and the combined organic layers were evaporated under reduced pressure. The residue was poured into ice water, and pale yellow solid of 8-formyl-7-hydroxy-4-methyl-coumarin was obtained. The further purification was carried out by
75 recrystallization with hot ethanol to obtain a light yellow powder (612.1 mg, Yield 10%). M.p. 180~181.0 ^{o}C (lit. 120.0~122.0 ^{o}C). ^{1}H NMR (300 MHz, CDCl$_3$): δ=12.22 (s, 1H); 10.62 (s, 1H); 7.74 (d, 1H, J = 9 Hz); 6.92 (d, 1H, J = 9 Hz); 6.21 (s, 1H); 2.43 (s, 3H). TOF MS EI calcd 204.0, found 204.0.

80

Synthesis of compound CHC

8-formyl-7-hydroxy-4-methyl-coumarin (408 mg, 2 mmol) was added into a solution of aqueous hydrazine (85%, 0.1 mL, about 2 mmol) in methanol (20 mL). Then the mixture was refluxed for
85 4 h. After completion of the reaction, the obtained yellow precipitate was filtered and washed several times with cold ethanol to give CHC (347 mg) as pure yellow solid in 86% yield. ^{1}H NMR (300 MHz, DMSO-d_6): δ=12.78 (s, 1H), 8.40 (s, 1H), 7.54 (d, J = 9.0 Hz, 1H), 6.87 (d, J = 9.0 Hz, 1H), 6.19 (s, 1H),
90 2.38 (s, 3H); ^{13}C NMR (75 MHz, DMSO-d_6) δ 160.69, 160.01, 154.43, 151.21, 135.49, 125.67, 113.33, 112.13, 110.85, 107.22, 18.80. ESI-HRMS: calcd. for (C$_{22}$H$_{16}$N$_2$O$_6$–H)$^-$ m/z 403.0930, found (M–H)$^-$: 403.0791.

95 ### Synthesis of compound CHN

Solution of 1-(hydrazonomethyl)naphthalene-2-ol (2) (186 mg, 1 mmol) and 7-hydroxy-4-methyl-2-oxo-2H-chromene-8-carbaldehyde (204 mg, 1 mmol) in 20 mL of ethanol was refluxed for 4 h. After completion of the reaction, the obtained yellow
100 precipitate was filtered and washed several times with cold ethanol to give CHN (346 mg) as pure yellowish solid in 93% yield. ^{1}H NMR (300 MHz, DMSO-d_6) δ 12.54 (s, 1H), 12.51 (s, 1H), 9.96 (s, 1H), 9.34 (s, 1H), 8.65 (d, J = 8.5 Hz, 1H), 8.02 (d, J

= 9.0 Hz, 1H), 7.89 (d, J = 7.8 Hz, 1H), 7.78 (d, J = 9.0 Hz, 1H), 7.60 (t, J = 7.5 Hz, 1H), 7.42 (t, J = 7.5 Hz, 1H), 7.24 (d, J = 9.0 Hz, 1H), 7.01 (d, J = 8.9 Hz, 1H), 6.26 (s, 1H), 2.39 (s, 2H); ^{13}C NMR (126 MHz, DMSO-d$_6$) δ 163.58, 162.61, 160.94, 159.58, 158.06, 154.31, 135.80, 133.49, 132.83, 130.42, 129.41, 128.65, 128.37, 124.39, 122.54, 119.24, 114.03, 112.48, 111.37, 108.88, 105.98, 518.80; ESI-HRMS: calcd. for $(C_{22}H_{16}N_2O_4–H)^-$ m/z 372.1032, found (M–H)$^-$: 371.2560.

Preparation of Samples

Preparation of nanoparticles

CHC or CHN of DMSO solutions (10 μL, 1×10^{-3}M) were rapidly injected into 2 mL of DMSO/H$_2$O mixtures of different ratios respectively with vigorous stirring at room temperature. The nanoparticles, with both of the concentrations 5μM (represented by the concentration of monomer, and it means the same hereinafter), were taken for fluorescence emission spectra and UV-visible absorption respectively.

Preparation of Samples for TEM Images

The nanoparticles were deposited on a 300-mesh copper grid coated with carbon, and observed at an accelerating voltage of 200kv in the condition of room temperature.

Preparation of Samples for Fluorescence Microscope Images

A drop of CHC or CHN nanoparticles suspension was dropped to a glass slide, and then covered with a coverslip. The excitation wavelength was set at 405 nm, choosing suitable filters.

Cell culture

HeLa cells were cultured in Dulbecco's modified Eagle's medium (DMEM) containing 10% fetal bovine serum and antibiotics (100 units/mL penicillin and 100 μg/mL streptomycin), maintaining at 37 ˚C in a humidified atmosphere of 95% air and 5% CO$_2$.

Cell imaging

Fresh stock of HeLa cells was seeded into a glass bottom dish with a density of 1×10^{-5} cells per dish, and incubated for 24 h. Subsequently, the cells were incubated with 5μM CHC or CHN nanoparticles in DMEM solution (adding 100 μL 10^{-3}M DMSO concentrated solution CHC or CHN to 1900 μL DMEM) for 4 h at 37 ˚C. Afterwards, the cells were washed three times with PBS to remove nanoparticles attached to the surface of cells and then fixed with 4% paraformaldehyde for 10 min at room temperature. The cells were imaged under confocal laser scanning microscopy (Olympus, FV-1000; λ$_{ex}$=405nm; fluorescent signals were collected at 420-700 nm for CHC and 430-650 nm for CHN). The images were captured using a photomultiplier.
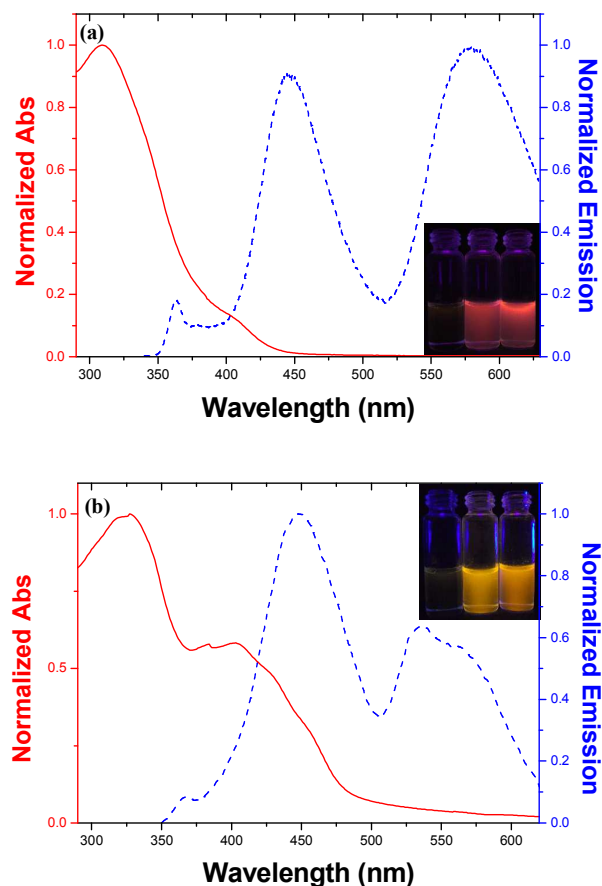
Results and Discussion

Fig. 1 Normalized absorption (solid line) and emission (dashed line) spectra of CHC nanoparticles in water/DMSO (v/v, 9/1) mixture (a) and CHN nanoparticles in water/DMSO (v/v, 7/3) mixture (b). Inert: photographs of CHC (a) and CHN (b) with concentration both of 5×10^{-5} M in DMSO dilute solution (left) and in water/DMSO mixture (middle, v/v, 1/1; right, v/v, 9/1) under 365 nm irradiation.

Both of CHC and CHN were soluble in common organic solvents, but insoluble in water. Hence, we employed a simple reprecipitation method without surfactants to obtain CHC and CHN nanoparticles. The molecularly dissolved dilute DMSO solutions of CHC and CHN were transparent, emitting very weak fluorescence which can hardly be observed (left of the two inert pictures). After the addition of water, as the formation of nanoparticles, reddish orange fluorescence of CHC nanoparticles (middle and right of Fig. 1a) and saffron yellow fluorescence (middle and right of Fig. 1b) of CHN nanoparticles could be observed by naked eye. The molar absorptivities for these two compounds as aggregates were 2.77×10^4 (CHC, λ$_{max}$=335 nm) and 2.14×10^4 (CHN, λ$_{max}$=340 nm) respectively. Those nanoparticles suspensions were transparent without precipitation and were observed to be stable even after a month. As shown in the normalized absorption and emission spectra of CHC

nanoparticles and CHN nanoparticles, large stokes shifts of ~270 nm for CHC nanoparticles and ~240 nm for CHN nanoparticles could be detected. Moreover, the quantum yield of the CHC (as aggregates) was 0.827 and the quantum yield of CHN (as aggregates) was 0.546, (using quinine as the reference with a known Φ value of 0.577 in 0.05 M H_2SO_4), indicating the great properties of CHC and CHN acting as solid state light-emitting materials.
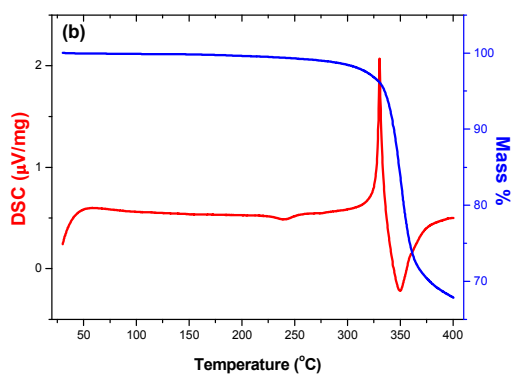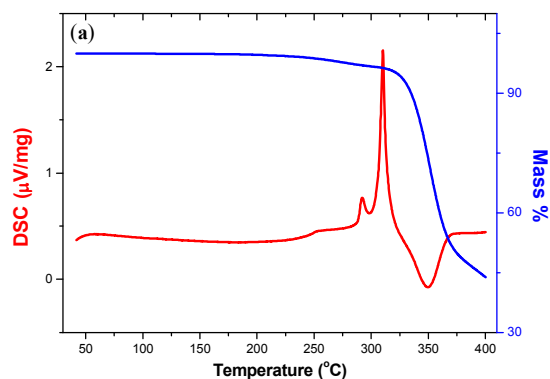
Thermal Stability Tests

Fig.2 DSC and TG curves of CHC (a) and CHN (b)

The thermal stabilities of CHC and CHN compounds were investigated by differential scanning calorimetry (DSC) and thermal gravimetric analysis (TGA). Fig.2 showed that the decomposition temperatures of CHC and CHN were both over 300℃, demonstrating their thermally stable properties.

Observation of CHC and CHN Nanoparticles

TEM Observation

Transmission electron microscope (TEM) images were obtained to observe the shape and size of the nanoparticles. TEM image in

Fig.3.a showed the CHC nanoparticles were claviform particles with a mean length of 500 nm. While as shown in Fig.3.b, the CHN nanoparticles were fine spheres with the diameters ranging from 60 to 100 nm.

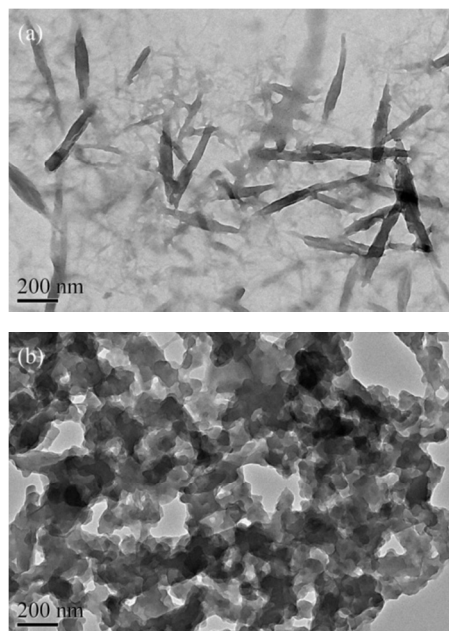Fig. 3 Transmission electron microscope (TEM) images of CHC (a) and CHN (b) nanoparticles obtained from suspensions of water/DMSO mixture

Fluorescence Microscope Images
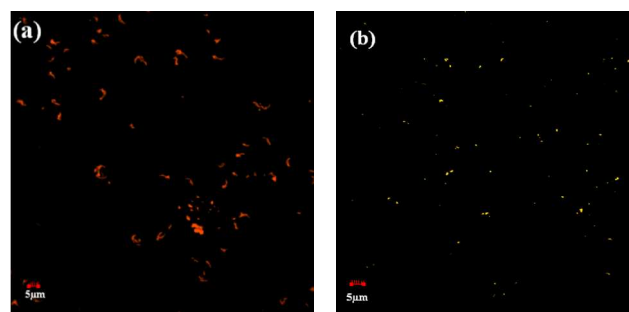
Fig. 4 Fluorescence microscope images of CHC (a) and CHN (b) nanoparticles (water/DMSO=7/3, v/v)

The fluorescence microscope images of CHC and CHN were shown in Fig.4a and Fig.4b. Upon excitation at 405 nm, CHC nanoparticles emitted reddish orange fluorescence, and the observed claviform shape fits in the TEM method. And for CHN, a large number of fluorescent dots emitting light could be observed. Additionally, the mean length of the CHC fluorescent bodies was 3μm, and the diameter of CHC fluorescent bodies was 1μm. Both were larger than the sizes observed by TEM which could be ascribed to the diffusion of light. Accordingly, the mutual authentication of fluorescent images and the TEM images

confirmed the existence of the CHC and CHN particles further.

Aggregation-induced emission Phenomenon

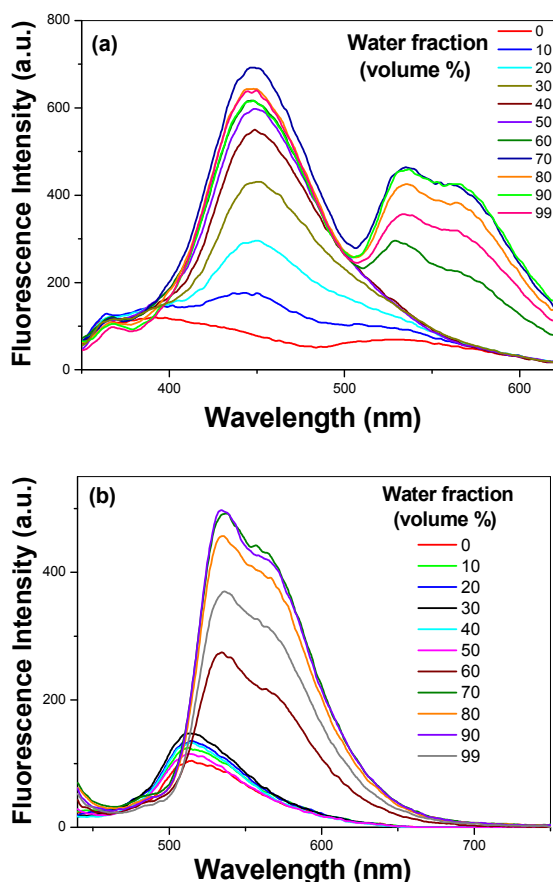Fig. 5 Fluorescent spectra changes of CHN (5×10^{-6}M) depending on the volume fraction of water in DMSO, λ_{ex}=323 nm (a) and λ_{ex}=416 nm (b).

The fluorescence spectra of CHN nanoparticles in water/DMSO with various ratios (keeping the concentration 5×10^{-6} M) upon excitation at 323 nm and 416 nm were shown in Fig. 5 respectively. As for the excitation at 323 nm, CHN in DMSO solution without water showed two weak peaks at 392 and 529 nm. In this situation, CHN molecules existed in the isolated state. Because of the free rotations of C-N single bonds, the ground state molecules could form a board range of torsional angle, from planer to twisted. So, this state were expected to have no emission due to the nonradiative decay processes through molecular torsions and rotations.[17] However, different from the hypothetical condition, in the actual excited state, the existence of hydrogen bonds to some extent hinders the free rotations. What's more, the relatively high viscosity of DMSO solution also attributes to the restriction of intramolecular rotation (RIR).[28] As a result, a weak and broad emission formed due to the restriction of intramolecular rotation, the enhancement of planarity, and the improvement of conjugation.

As the water fraction increased, a new emission peak located at

447 nm appeared. The fluorescence intensity enhanced gradually namely the AIE characteristic of CHN, indicating the formation of aggregated nanoparticles. This enhancement was depicted in Fig. 6a. At the long wavelength region, when the fraction of water increased to 60%, an emission peak located at 534 nm appeared, with a shoulder emission peak at 565 nm. The fluorescent intensity values of the three peaks all reached the maximum (Φ_F=0.546) in the condition of 70% water exists.

The enhanced fluorescence emission could be explained in terms of the intra- and intermolecular effects. CHN molecule consists of an N-N moiety as a bridging group. Rather than the free rotation in isolated state, a more planar conformation was favored in the aggregation state. Hence the non-radiative decay could be prevented. Therefore, the conformational changes relating to the rotation of the N-N moiety played an important role on the AIE.

And also, it was probably that the aggregation-induced planarizations inevitably induced the intermolecular interactions. It is widely acknowledged that the formation of excimer complex, which can be ascribed to the strong intermolecular interactions of planar π-conjugated in the solid state, leads to the fluorescence quenching.[8] However in CHN, the bulky and polar hydroxy group restricts the parallel face-to-face intermolecular interactions in the aggregated state, namely the H-aggregate formation which exhibits blue-shifted absorption bands compared to the isolated state.[17] The prevention of H-aggregation forces the head-to-tail aggregation, the J-aggregation, which induces a great enhancement in fluorescence. The absorption spectra of CHN in isolated state and aggregated state, shown in Fig. S1, were also accord with the bathochromic shift in absorption maximum of J-aggregation.

Therefore, most probably, the fluorescent enhancement of CHN could be ascribed to the combined effects of aggregations-induced planarization and J-aggregate formation.

After the water fraction increased to 70%, the fluorescence intensities decreased as further increase of the water fraction. This emission decreases could be explained by the change in the shapes of the aggregates. When the water fraction was lower than 70%, the molecules accumulate slowly in an ordered way to form more emissive nanoparticles.[12] Whereas in a system of higher water fraction, the CHN molecules agglomerated quickly in a random way to form amorphous nanoparticles less emissive. Concerning the emission spectra upon excitation at 416 nm shown in Fig. 5b, conditions were similar as excitation at 323 nm for the long wavelength region. However, no emission peak in the short wavelength region can be observed. As for the CHC nanoparticles, conditions were similar except the specific water fractions, and they were depicted in Fig. 7.
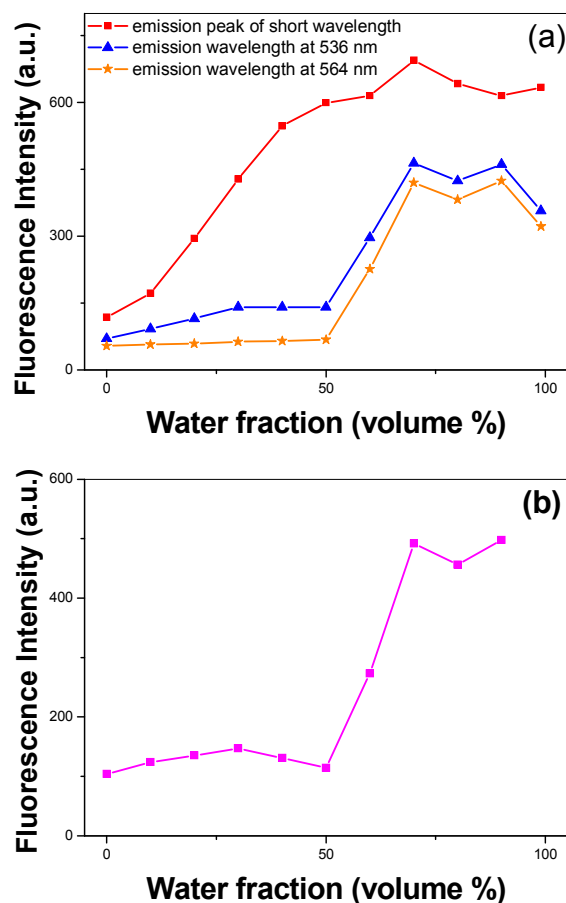
Fig. 6 Variation in the fluorescence intensity at different emission peaks of CHN with the increasing volume fraction of water in DMSO, λ_{ex}=323 nm (a) and λ_{ex}=416 nm (b).
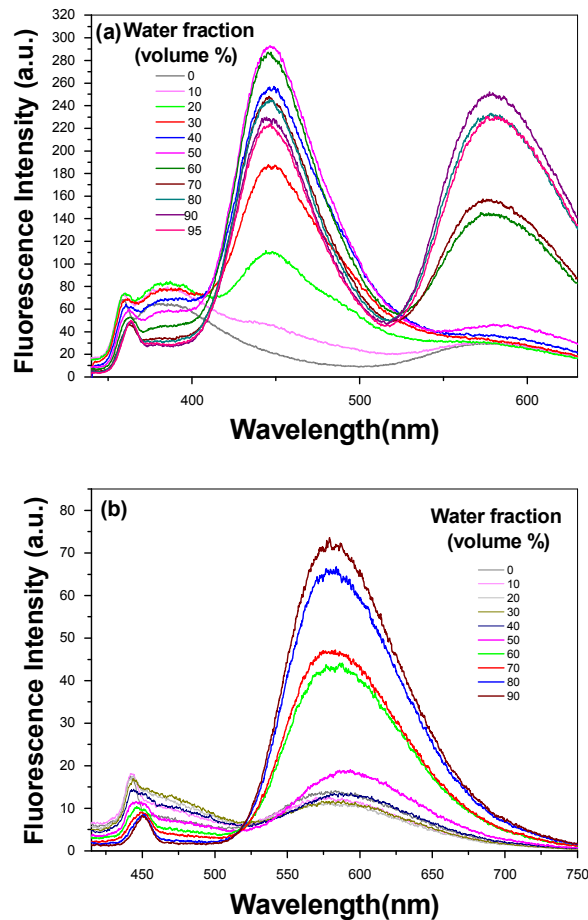

Fig. 7 Fluorescent spectra changes of CHC (5×10^{-6}M) depending on the volume fraction of water in DMSO, λ_{ex}=323 nm (a) and λ_{ex}=390 nm (b).

Investigation of the contribution of ESIPT to fluorescent emission features

In order to verify whether proton-transfer existed and how it impacted on the excited state of CHC and CHN, we measured the FL spectra in solvents with different polarities. At the same concentration, we noticed that the emission intensities decreased with the increase of the polarities of the solvents, as shown in Fig. S2, because these two ESIPT compounds could form intermolecular H-bonds with protic or polar solvents.[29] Thus this phenomenon indicated the existence of the ESIPT process to some extent.

The basic process of the ESIPT has been illustrated in a large number of literatures,[30] and a brief introduction of ESIPT is shown in Fig. 8.a. In the ground state, the enol form (E) was more stable than the keto form (K). Upon photoexcitation, ESIPT occured on an fs-timeacsle, transforming the excited enol form (E*) to the excited proton-transferred keto form (K*) which was preferred in the excited state. Then, the excited keto form (K*)

relaxed radiatively to the ground-state keto form (K) releasing a large Stokes-shifted fluorescence. Finally, the ground-state keto form (K) transformed to the original enol form (E) in the ground. It is widely acknowledged that ESIPT only occurs through planar

5 structure because of an increasing ESIPT barrier correlating with the twist angle.[31] On the basis of molecular structure, it had a twisted structure at the energetic minimum of the ground state; while on the other hand, a planar structure was more stable in the excited state. Hence, the transition energy gap of planar

10 molecules was lower. Therefore, the long wavelength photons, 416 nm for CHN and 390 nm for CHC in our experiment, exclusively excite planar or near-planar molecules, and the proton transfer took place right after excitation leading to none short wavelength region emission observed. At short wavelength, 323

15 nm in our experiment, all molecules were excited. For the planar molecules, the ESIPT process could occur directly. However, for the twisted molecules, the increased barrier enforced the molecules to planarize first before proton-transfer. Therefore, the fluorescence spectra are closely related to the molecular

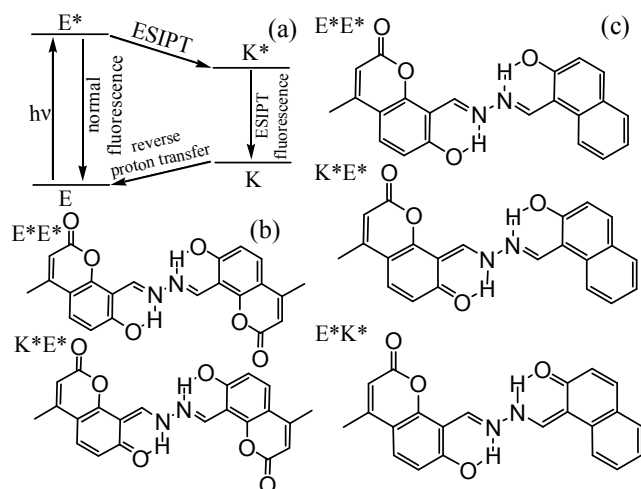20 population and reaction rate of ESIPT.

Fig. 8 Mechanism of ESIPT process (a). Excited-state tautomers for CHC (b) and CHN (c).

25

Concerning our fluorescence spectra of CHN upon excitation at 323 nm, as the increase of water fraction, the ratio of planar molecules rises as the nanoparticles form. After the water fraction increases to 60%, the ESIPT emission peak could be observed.

30 Based on the discussion above, nanoparticles of CHN namely the planar molecules were expected to emit three maximum peaks coming from E*E*, E*K* and K*E* tautomers respectively. The emission maximum peak at 447 nm, with a small Stokes shift and mirror-image shape, could be ascribed to the radiative decay from

35 the E*E*. As for the two emission maximum peaks in the long wavelength region, the large Stokes shifts indicated they are originated from E*K* and K*E* tautomers separately. The ESIPT emission peak of phenolic OH on 2-hydroxy-1-naphthaldehyde to nitrogen atom had been reported to be located

40 at 531 nm.[32] And the fluorescence spectra of CHC nanoparticles which only had a single ESIPT emission peak coming from E*K*

tautomers, shown in Fig. 7, revealed the ESIPT emission peak of phenolic OH on 8-Formyl-7-hydroxy-4-methyl-coumarin to the nitrogen atom appeared at 570 nm. Accordingly, emission peak at

45 534 nm could be assigned to E*K* species and the other emission peak at 565 nm probably came from K*E* species.
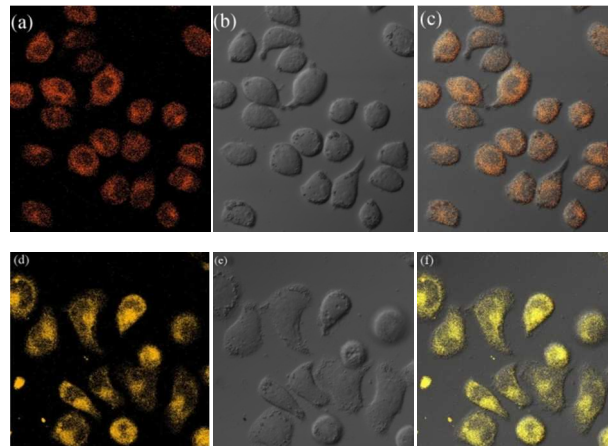
Cell staining

50

Fig. 9 Confocal microscopy images of cells incubated with 5 µM nanoparticles solution for 4 h, upon excitation at 405 nm. CHC: (a) excited with 405 nm laser. (b) Bright field image. (c) Merger of a and b.

55 CHN: (d) excited with 405 nm laser. (e) Bright field image. (f) Merger of d and e.

Cell permeability enabled the compounds to enter living cells hence further intracellular investigations became possible. To test

60 whether CHC and CHN could enter cells and served as biological fluorescence probes, HeLa cells were incubated with CHC and CHN nanoparticles and then examined by fluorescence confocal microscopy. As shown in Fig. 9, HeLa cells incubated with nanoparticles solution was excited by 405 nm, and emitted

65 reddish orange fluorescence stained with CHC, saffron yellow fluorescence stained with CHN. The merged image revealed that fluorescence could only be detected inside the HeLa cells instead of a random position. Therefore, CHC and CHN could be assimilated by HeLa cells and aggregates in their cytoplasm.

70 Moreover, cell morphology remained in fine condition after intake of the nanoparticles, indicating the great cytocompatibility of CHC and CHN. The biological imaging tests on HeLa cells have shown that both of CHC and CHN had good photophysical properties and could be good candidates for cell staining avoiding

75 the impacts of excitation light.

Conclusions

In summary, we have designed and synthesized two coumarin-based fluorescent molecules CHC and CHN. The two compounds

80 are stable and show high thermal stabilities. In addition, the ESIPT fluorescence could be utilized as a new strategy to develop other AIE-active materials. The success of coumarin-based series is expected to accelerate organic photo-material discovery and lead to further technological applications in the fields of

nanobiotechnology and optoelectronics, and potential uses in cell imaging.

Notes and references

1 (*a*) Y. Liu, X. T. Tao, F. Z. Wang, X. N. Dang, D. C. Zou, Y. Ren and M. H. Jiang, *J. Phys. Chem.* C, 2008, **112**, 3975; (b) Doi, H.; Kinoshita, M.; Okumoto, K.; Shirota, Y. Chem. Mater. 2003 , 15 , 1080; (c) C. L. Chiang, M. F. Wu, D. C. Dai, Y. S. Wen, J. K. Wang and C. T Chem, *Adv. Funct. Mater*, 2005, **15**, 231.

2 X. G. Yu, J. S. Yu, J. L. Zhou, W. Huang and H. Lin, *Eur. Phys. J. Appl. Phys.*, 2013, **62**, 20101.

3 (*a*) F. Y. Yan, M. Wang, D. L. Cao, N. Yang, Y. Fu, L. Chen, L. G. Chen, *Dyes and Pigments*, 2013, **98**, 42; (*b*) W. T. Gong, B. Gao, S. Bao, J. W. Ye, G. L. Ning, *J Incl Phenom Macrocycl Chem*, 2012, **72**, 481.

4 H. Anders, G. Michael, *Chem. Rev.*, 1995, **95**,49.

5 M. Xavier; P. Fabien; L. Thilo D.; D. Maxime; B. Marcel P.; A. A. Paul; W. Shimon, Single Molecules, 2001, **2**(4), 261.

6 Recent advances in solid-state organic lasers Polymer International Polym Int 2012;61: 390 – 406

7 (*a*) S.A. Jenekhe, J.A. Osaheni, *Science*, 1994, **265**, 765; (*b*) J. Malkin, *Photophysical and Photochemical Properties of Aromatic Compounds*, CRC, Boca Raton, 1992; (*c*) N. J. Turro, *Modern Molecular Photochemistry*, University Science Books, Mill Valley, 1991; (*d*) X. C. Li and S. C. Moratti, in *Photonic Polymer Systems*, ed. D. L. Wise, G. E. Wnek, D. J. Trantolo, T. M. Cooper and J. D. Gresser, Marcel Dekker, New York, 1998, ch. 10.

8 J. B Birks, *In Photophysics of Aromatic Moelcules*, Wiley, London, 1970.

9 (*a*)W. Z. Yuan, P. Lu, S. M. Chen, Jacky W. Y. Lam, Z. M. Wang, Y. Liu, H. S. Kwok, Y. G. Ma and B. Z. Tang, *Adv. Mater.*, 2010, **22**, 2159; (b) Y. T Lee, C. L. Chiang and C. T. Chen, *Chem. Commun.*, 2008, 217; (*c*) C. W. Wu, C. M. Tsai and H. C. Lin, *Macromolecules*, 2006, **39**, 4298; (*d*) J. Wang, Zhao, Y. C. Dou, H. Sun, P. Xu, K. Ye, J. Zhang, S. Jiang, F. Li and Y. Wang, *J. Phys. Chem. B*, 2007, **111**, 5082; (*e*) F. He, Y. Tang, S. Wang, Y. Li and D. Zhu, *J. Am. Chem. Soc.* , 2005, **127**, 12343; (*f*) S. Hecht and J. M. J. Frechet, *Angew. Chem., Int. Ed.*, 2001, **40**, 74.

10 J. Luo, Z. Xie, J. W. Y. Lam, L. Cheng, H. Chen, C. Qiu, H. S. Kwok, X. Zhan, Y. Liu, D. Zhu and B. Z. Tang, *Chem. Commun.*, 2001, 1740.

11 (*a*) S. J. Li, B. K. An, S. D. Jung, M. A. Chung and S. Y. Park, *Angew. Chem., Int. Ed.*, 2004, **43**, 6346; (*b*) B. K. An, S. K. Kwon, S. D. Jung and S. Y. Park, *J. Am. Chem. Soc.*, 2002, **124**, 14410.

12 (*a*) H. Tong, Y. Dong, M. Haussler, J. W. Y. Lam, H. H. Y. Sung, I. D. Williams, J. Sun and B. Z. Tang, *Chem. Commun.*, 2006, 1133; (*b*) H. Tong, Y. Dong, Y. Hong, M. Haussler, J. W. Y. Lam, H. H. Y. Sung, X. Sun, J. Yu, I. D. Williams, H. S. Kwok and B. Z. Tang, *J. Phys. Chem. C*, 2007, **111**, 2287.

13 B. Zhang, W. Diao, C. Bi, J. Sun, G. X. Han, Y. Shi, L. Sheng, G. Yin and L. Pu, *J Fluoresc*, 2012, **22**, 1.

14 (*a*) Y. Q. Li, R. T. K. Ryan, B. Z. Tang, B. Liu, *RSC Adv*, 2013, **3**(26), 10135; (*b*) S. Mukherjee and P. Thilagar, *Chem. Commun.*, 2013, **49**, 7292.

15 (*a*) X. Y. Zhang, X. Q. Zhang, B. Yang, M. Y. Liu, W. Y. Liu, Y. W. Chen and Yen Wei, *Polym. Chem.*, 2013, **4**, 4317; (*b*) H. H. Lin, Y. C. Chan, J. W. Chen and C. C. Chang, *J. Mater. Chem.*, 2011, **21**, 3170.

16 A. Hagfeldtt, M. Gratzel, *Chem. Rev.*, 1995, **95**, 49.

17 (*a*) D. Oelkrug, A. Tompert, H. Egelhaaf, M. Hanack, E. Steinhuber, M. Hohloch, H. Meier, U. Stalmach, *Synth. Met.*,1996, **83**, 231; (b) D. Oelkrug, A. Tompert, J. Gierschner, H. Egelhaaf, M. Hanack, M.

Hohloch, E. Steinhuber, *J. Phys. Chem. B*, 1998, **102**, 1902. (*c*) M. M. Souza, G. Rumbles, I. R. Gould, H. Amer, I. D. W. Samuel S. C., Moratti, A. B. Holmes, *Synth. Met.*, 2000, **111-112**, 539.

18 W. I. J. Gruszecki, *Biol. Phys.*, 1991, **18**, 99.

19 V. V. Shynkar, A. S. Klymchenko, E. Piemont, A. P. Demchenko and Y. Mely, *J. Phys. Chem. A*, 2004, **108**, 8151.

20 K. Sakai, T. Tsuzuki, Y. Itoh, M. Ichikawa and Y. Taniguchi, *Appl. Phys. Lett.*, 2005, **86**, 081103.

21 F. S. Liang, L. X. Wang, D. G. Ma, X. B. Jing and F. S. Wang, *Appl. Phys. Lett.*, 2002, **81**, 4.

22 A. P. Dalmau, *J. Org. Chem.* , 1995, **60**, 5468.

23 D. Y. Chen, C. L. Chen, Y. M. Cheng, C. H. Lai, J. Y. Yu, B. S. Chen, C. C. Hsieh, H. C. Chen, L. Y. Chen, C. Y. Wei, C. C. Wu and P. T. Chou, ACS *Appl. Mater. Interfaces*, 2010, **2**, 1621.

24 A. Z. Weller, *Elektrokhimiya*, 1956, **60**, 1144.

25 (*a*) H. Tong, M. HäuBler, Y. Q. Dong, Z. Li, B. X. Mi, H. S. Kwok, B. Z. Tang, *Journal of the Chinese Chemical Society*, 2006, **53**,243; (*b*) S. Li, L. He, F. Xiong, Y. Li, G. Yang, *J. Phys. Chem. B*, 2004, **18**, 10887; (*c*) X. Chen, R. Wei, Y. Xiang, Z. Zhou, K. Li, P. Song, A. Tong, *J. Phys. Chem. C*, 2011, **115**, 14353.

26 L. Jiang, L. Wang, M. Guo, G. Yin, R. Y. Wang, *Sensors and Actuators B*, 2011, **156**,825.

27 D. R Bender, D. Kanne, J. D. Frazier, H. Rapoport, *J. Org. Chem.*, 1983, **16**, 2714.

28 R. Hu, S. Y. Li, Y. Zeng, J. P. Chen, S. Q. Wang, Y. Li and G. Q. Yang, *Phys. Chem. Chem. Phys.*, 2011, **13**, 2044.

29 T. He, X. T. Tao, J. X. Yang, D. Guo, H. B. Xia, J. Jia, M. H. Jiang, *Chem. Commun.*, 2011, **47**, 2907.

30 (*a*) K. Ando, S. Hayashi, S. Kato, *Phys. Chem. Chem. Phys.*, 2011, **13**, 11118; (*b*) C. C. Hsieh, C. M. Jiang, P. T. Chou, *Acc. Chem. Res.*, 2010, **43**, 1364; (*c*) G. Y. Li, G.J. Zhao, Y. H. Liu, K. L. Han, G. Z. He, *J. Comput. Chem.* , 2010, **31**, 1759; (*d*) J. N. Li, M. Pu, D. C. Fang, M. Wei, J. He, D. E. Evans, *J. Mol. Struct.*, 2012, **1015**, 106; (*e*) G. Gui, Z. Lan, W. Thiel, *J. Am. Chem. Soc.*, 2012, **134**,1662.

31 T. Sekikawa, O. Schalk, G. R. Wu, A. E. Boguslavskiy and Albert Stolow, *J. Phys. Chem. A*, 2013, **117**, 2971.

32 X. Cao, X. Zeng, L. Mu, Y. Chen, R. X. Wang, Y. Q. Zhang, J. X. Zhang, G. Wei, *Sensors and Actuators B*, 2013, **177**, 493.

New Journal of Chemistry Accepted Manuscript

Two coumarin-based AIE-active compounds emitting ESIPT fluorescence with large Stocks-shifts were applied to cell imaging.